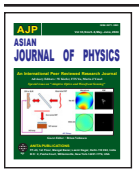

Asian Journal of Physics
Vol. 33, Nos 5 & 6 (2024) 349-368
Available on: www.asianjournalofphysics.com

ap

Null screens and corneal topography

Rufino Díaz-Uribe[1], Martín Isaías Rodríguez-Rodríguez[2], and Yobani Mejía[3]

[1]*Instituto de Ciencias Aplicadas y Tecnología, Universidad Nacional Autónoma de México, Apdo. Postal 70-186, México City, 104510, Mexico*

[2]*Facultad de Estudios Superiores Iztacala UNAM, Avenida de los Barrios No. 1 Col. Los Reyes Iztacala, Tlalnepantla Estado de México C.P. 54090, Mexico*

[3]*Departamento de Física, Universidad Nacional de Colombia, Bogotá, Colombia*

This paper presents a review of the null screen test method for measuring the anterior surface of the cornea. The paper is focused on the field curvature and the skew ray problem, both present in the specular topographers based on the Placido disc targets, and how they can be solved by the null screen method. The main issues related to this technique such as null-screen design, setup, quantitative evaluation methods and different target configurations used in experimental and commercial devices are reviewed. This review shows that the Null-Screen testing method has become an important tool for measuring the anterior surface of human corneas. © Anita Publications. All rights reserved.

doi: 10.54955.AJP.33.5-6.2024.349-368

Keywords: Optical Deflectometry, Null Screens, Corneal Topography.

1 Introduction

Corneal topography is a very relevant theme for opticians, ophthalmologists, and optometrists. A complete knowledge of the shape of the cornea as well as its optical power are essential, because of the monitoring and diagnostics of degenerative diseases.

There are several kinds of corneal topographers ranging from the classic Placido´s Disk specular reflection topographers which are able only to measure the anterior corneal surface to OCT passing through the diffuse reflection of a slit lamp beam together with the Scheimpflug camera which are able to measure also the posterior corneal surface, the corneal pachymetry and measure some other inner structures of the eye as the iris, the crystalline lens, among other.

Historically, the search for a method of measuring the shape of the cornea is an epic story of the science, the reader can browse some interesting documental sources that are out of the scope of the present paper [1]. Briefly, we start with the Placido´s Disk invented in 1880 by Antonio Placido da Costa, a Portuguese ophthalmologist at the end of the XIX century, bring to the ophthalmologists the opportunity to visualize the shape or the topography of the anterior surface of the cornea to find some deformations [1]. Later, in 1896, Alvar Gullstrand captured the reflected image with a photographic camera and was the first who proposed a method to quantify the shape of the cornea [2]; he called the method, *Photographic Ophthalmometry*. This remained with few changes until the appearance of personal computers and the ability to digitize images to be analyzed faster and accurate. At the end of eighties decade of the last century first commercial devices, called videokeratometers, appeared as new tools to diagnose some refractive diseases;

Corresponding author
e mail: rufino.diaz@icat.unam.mx (Rufino Díaz-Uribe)

EyeSys [3,4], Atlas from Zeiss [5], and Cornea from Essilor [6], are modern commercial examples of the now called specular reflection topographers based on Placido´s concentric rings. Later, during the next decade there appeared a new kind of device called ORBSCAN; soon it became the Gold Standard and prevailed for many years. Apart from using a target with a set of rings similar to the Placido´s Disk, the Orbscan projects a slit lamp beam and scan laterally on the cornea. This device allows to measure not only the topography of anterior but also of the posterior surface and the corneal thickness not only at one or few points, but also along a wide zone around the corneal vertex [7]. Then, other similar devices were developed; for instance, the Pentacam projects two slit beams to scan on the cornea by rotating them around the optical axis; now Pentacam has become the gold standard in corneal topography [8]. More recently, the OCT based on a low coherence beam to produce an interference pattern only when the test beam is diffusely reflected on a point object at practically the same distance of the mirror producing the reference beam, so the mirror gives accurately the object distance. The test beam must be scanned along the xyz directions to produce a 3D map of every point on the object to be measured [9]. The amount of information provided by a OCT is huge and its applications in many areas of medicine are growing every day [10]. Every kind of system has its own advantages and drawbacks. The powerful OCT is very complex and expensive to be used only as a corneal topographer. The scanning slit lamp beam systems use mechanical scanning methods which are slow for the eye and need an eye tracking device to compensate for the movements of the eye during the scanning; these systems are less expensive than OCT systems, but the simple reflection topographers are even the cheaper; they are enough for some clinical applications, as the contact lens fitting or for finding some ectasias affecting the anterior corneal surface.

This review describes the main issues related to the specular reflection based topographers and emphasize those based on the null screen methodology. In section 2, a paraxial analysis of the specular topographers is made. In section 3, the field curvature produced by different targets is described. In section 4, the well known skew ray problem of the Placido's Disk based topographers is explained and how it was solved. Then, the null screen method is introduced in section 5 and the basic theory used to evaluate the corneal topography. In section 6 the way that a null screen is designed is introduced, while in section 7 some methods to quantitatively evaluate the corneal topography are reviewed. Then, different variations of corneal topographers using the null screen method are described and in section 8 and in section 9 the Dynamic Point Shifting method (DyPoS) is explained. In section 10 the conclusions of this paper are enunciated.

2 Specular topographers

This kind of topographers make use of the image produced by the tear film covering the cornea, of real object called the target. Early topographers used a target like the Placido's Disk made of

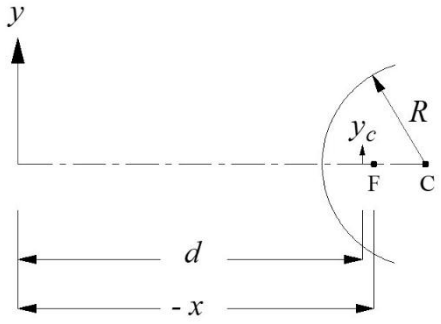

Fig 1. Virtual image of height y_c of an object of height y made by a spherical mirror. F is the focal point of the mirror and C its center of curvature. The Newtonian distance of the object is $-x$. The distance between the object and the image is d.

alternating bright and dark rings on a flat surface. For a quantitative evaluation of the cornea, the keratometric method was proposed to be applied on analog pictures of the image captured with reflex or even with instant Polaroid cameras. To see it, let us consider the Fig 1. A target (ring) of height y at a distance x from the focal point F of the spherical mirror of radius of curvature R has a virtual image of height y_c, separated from the object a distance d. In practice, the distances x and d are close together. The radius can be calculated as $R = 2dy_c/y$.

Let us consider a Placido's Disk as in Fig 2(a). The cornea forms a virtual image of the rings near its focal point, then the lens L forms a real image of these rings on the image plane (camera sensor), and they are seen as shown in Fig 2(b).

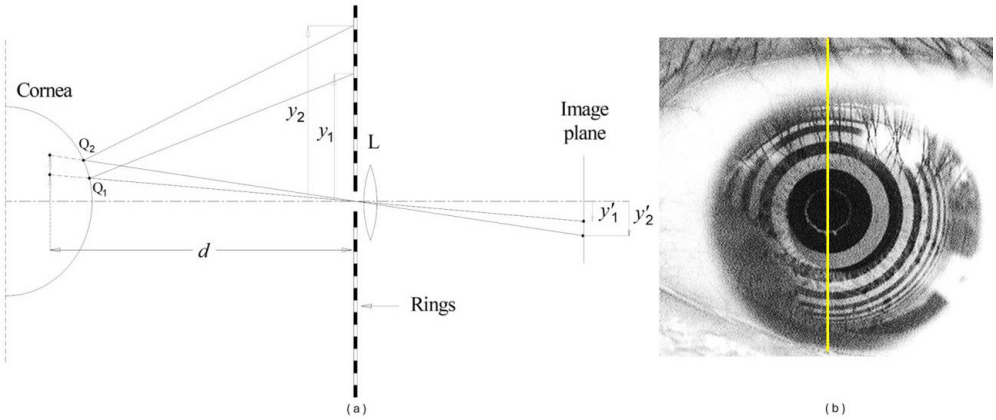

Fig 2. Measurement of corneal topography with a Placido's disc using a plane target. (a) A lens L made a real image of the virtual image of the rings. (b) Ring pattern and a meridional plane (yellow line) to measure y_1' or y_2' to calculate the radius of curvature at Q_1 or Q_2.

By measuring the radial distance of the rings on a meridional plane (yellow line in Fig 2(b)) the local curvature at any point Q on the cornea is determined. For instance, following the geometry of Fig 2(a), the radius of curvature at Q_1 and Q_2. are

$$R_1 = 2\,\frac{d}{m}\,\frac{y'_1}{y_1} \tag{1a}$$

and

$$R_2 = 2\,\frac{d}{m}\,\frac{y'_2}{y_2}. \tag{1b}$$

where m is the magnification of the lens L. As the image rings are distorted, $y'_1/y_1 \neq y'_2/y_2$, therefore the local radii are different. Then, a map of the corneal power (local radii) for different regions was evaluated. However, these measurements are made in the meridional direction.

Soon, two main problems were evident. The first one was the field curvature at the image, the second was the so called skew ray problem.

3 Field curvature

Even though the specular reflection topographers are the simplest, they had to solve some problems before they were accurate enough to be useful. May be the less complex is the field curvature that affects the virtual image produced by the spherical mirror (cornea) when the object is flat (Placido's Disk); the photographic cameras are designed to capture images of plane objects orthogonal to the optical axis of the

objective lens of the camera; for a plane real object as the Placido's Disk, the image produced by reflection on a convex spherical surface, which approximates to the anterior corneal surface, lies on a virtual curved surface inside the cornea, which is the first Purkinje image, Fig 3.

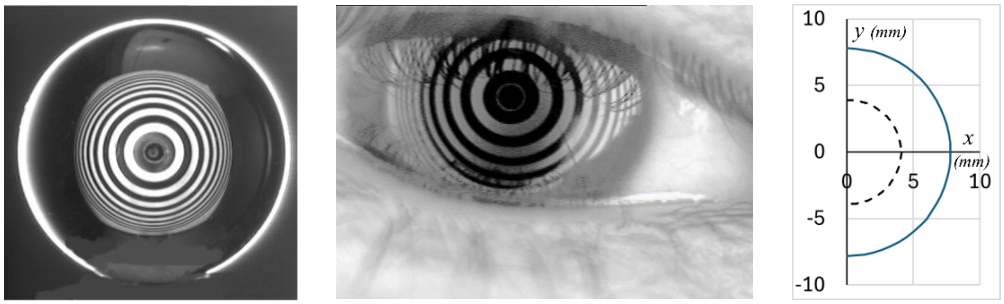

(a) (b) (c)

Fig 3. Image of a flat Placido's Disk observed by reflection on a 1/2 inch diameter steel ball (a) and on a real human cornea (b). The field curvature on the image is evident. (c) Image surface (dotted line) produced by a 7.8 mm radius of curvature sphere (blue line) with a plane object located 100 mm at the right of its vertex as calculated from the parabasal approximation.

Parabasal calculations show that a good approximation to the shape of image surface produced by a flat Pacido's disk located at a distance x_o from the origin at the center of a sphere of radius of curvature R, is an ellipsoid of revolution, whose symmetry axis is the normal to the plane object passing through the center of the sphere. The ellipsoid satisfies the canonical equation

$$\frac{(x_i - x_c)^2}{a^2} + \frac{y_i'}{b^2} = 1 \tag{2}$$

where x_i, y_i are the cartesian coordinates of the points on the image surface; 2a, and 2b are the corresponding major and minor axes of the ellipse along the x and y axes, which can be written as

$$a = \frac{Rx_o}{\sqrt{4x_o^2 - R^2}} \text{ and } b = \frac{2Rx_o^2}{4x_o^2 - R^2} \tag{3}$$

Finally, the center of the ellipse representing the image surface is displaced from the origin along the x-axis a distance x_c, which is given by

$$x_c = \frac{R^2 x_o}{4x_o^2 - R^2} \tag{4}$$

By the same argument, and considering that the object and the image are optical conjugates, it can be shown that the object surface whose image is a plane, nearly correspond to an ellipsoid of revolution [11]. Based on the Coddington Equations Mejía-Barbosa [12] showed that, two image surfaces can be found; one for the meridional or tangencial rays, the other for the sagittal rays; strictly none of them are ellipsoids, they called ovoid surfaces, but they are close to the ellipsoid described before. Any way, it is also true that the real object surface producing a virtual plane image to be captured by a photographic camera is an ovoid surface, nearly an ellipse of revolution. As far as we know, Mejía-Barbosa has been the only one to construct such an ovoid object surface [12].

As was stated above, for a flat object as the Placido's Disk, the image produced by reflection on a convex spherical surface, which approximates to the anterior corneal surface, lies in a virtual curved surface inside the cornea, which generates a blurring effect in the image that increases as the point object on the target moves away from the optical axis. Moreover, as the luminous sources on the rings are located far

from the optical axis, an aberration called astigmatism is observed. The spherical mirror will image a point source on a plane as a short segment perpendicular to the tangential plane. By moving away the plane from the vertex of the spherical mirror the image changes from the segment to a small circle, called the circle of least confusion, and then to another short segment perpendicular to the sagittal plane. Then, if we image the whole flat object, we get three surfaces (astigmatic surfaces). The surface where the tangential rays are in focus is called the surface T, and the surface where sagittal rays are in focus is called the surface S. In the middle of T and S surfaces there is the surface M where we have the circle of least confusion [12].

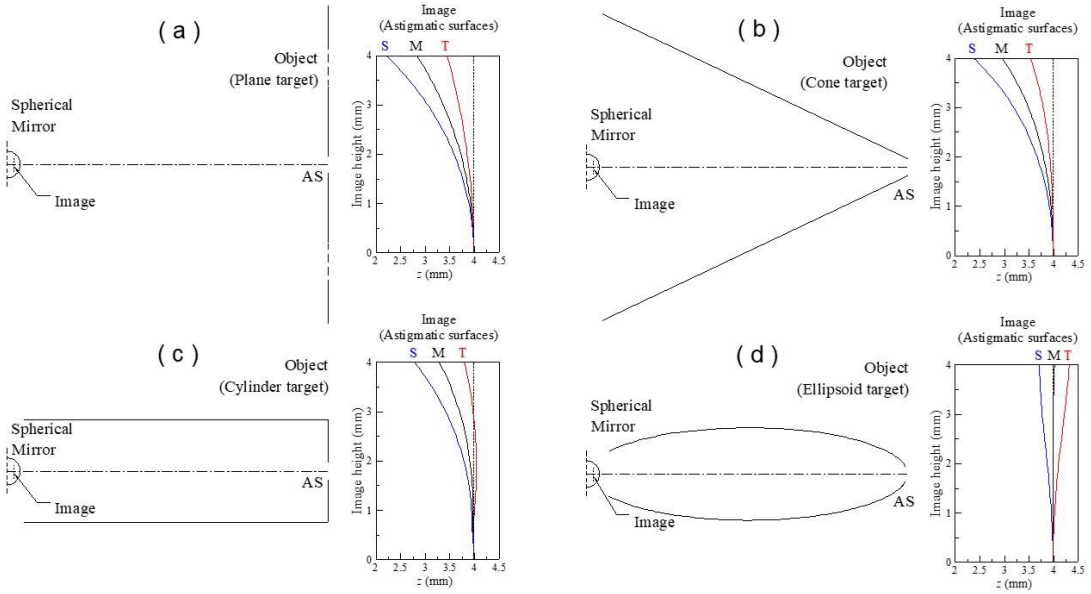

Fig 4. Some targets and their corresponding astigmatic curves.

In Fig 4(a), we show the astigmatic curves (in a meridional plane) made by a spherical mirror of radius of curvature $R = 7.8$ mm when the flat object is 180 mm away from the mirror. The dashed line in the plot corresponds to the Gaussian image plane, which is at 3.98 mm from the center of curvature of the mirror. To get an image of height 4 mm, we need a flat object of height about 340 mm. In other words, to test a circular region on the cornea of 4 mm of radius, we need a big Placido´s Disk of about 680 mm of diameter. If we reduce the diameter of the disk the interest region on the cornea is also reduced. One way to overcome it was done by replacing the disk by a cone, as shown in Fig 4(b). However, the astigmatic curves do not change a lot, and the blurring effect is almost the same as the one in the Placido's Disk. An improvement is achieved by using a cylinder target as in Fig 4(c). The astigmatic surface T is flattened, and astigmatic surfaces M and S are closer to the gaussian image plane. An additional improvement can be achieved by using an ellipsoid target as in Fig 3(d). In this case the astigmatic surface M has been flattened. It is an ideal target if we consider that the best image of a point source must be a circular spot, i.e. the circle of least confusion. However, the manufacture of this type of screens is not simple. In practice, a cylindrical target is an easy solution. In the last three cases, (b), (c), and (d), we have used the same spherical mirror and the same location for the aperture stop AS used in (a). In (b) the base of the cone is of 188 mm of diameter, in (c) the length of the cylinder is also 180 mm, and in (d), for the ellipse, the major axis is 180 mm, and the minor axis is 54 mm. The calculations of the astigmatic surfaces in all cases have been done using the Coddington equations [12].

4 Skew ray problem

As it was stated before, a first approximation to the evaluation of a corneal surface is given by the method of a keratometer Eq (1). This equation, however, is only valid in the paraxial regimen, i.e., for small objects located close the optical axis, and rays incident within a small area around the vertex. The use of this equation far beyond these limits will give wrong results. In an attempt to fix this problem, non paraxial approximations were used but maintaining their calculations in the meridional plane since the works of Gullstrand [2], passing through several meridional evaluation schemes [13] until recent years when the skew ray problem was identified [14,15]. During many years prevail the false idea that for evaluating the corneal topography using the Placido's Disk or concentric rings target, just locate the center of the rings on the image and use it as a starting point for measuring the radial separations of the image rings. For surfaces with symmetry of revolution and well aligned systems, this is correct, but for non-symmetric surfaces or even for axially symmetric surfaces but misaligned systems, this method is not correct.

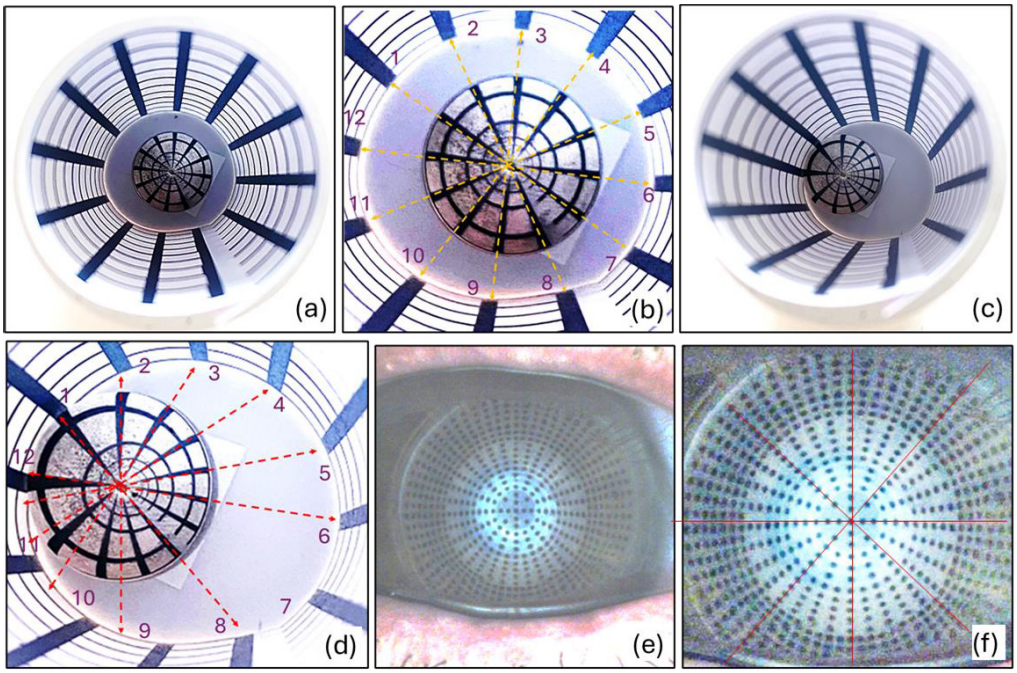

Fig 5. A spherical steel ball is located inside a cylindrical target with straight lines parallel to the z axis; z is the cylinder axis of symmetry. The target also has a set of orthogonal rings to z axis; r and q complete the cylindrical coordinates. (b) Detail of (a), the rings on the target are defined by ($z = z_j$; $j = 1, 2, \ldots$), but only five are clearly visible on the ball; the straight lines are defined by $r = R$, and $q = q_k$; $k = 1,\ldots,$ 12. The sphere is at the center of the cylinder; the image of the rings observed by reflection on the sphere are the concentric circles while the radial straight lines on the image are due to the parallel straight lines at the target; the image of lines 1, 2,...6 are continued along the image of lines 7, 8,…,12, correspondingly; in this case, the image of any straight line on the target belongs to a single meridional plane of the surface. (c) The same sphere is displaced from the center. (d) Detail of (c), showing that the image is deformed as compared to (b); on the image, some of the radial lines are no longer straight lines and the circles are deformed and not concentric. Furthermore, apparently the image of 1 is a continuation of the opposite, but line 8 is not the opposite of line 1 in the target; in addition, some radial images have no continuation as in (b); lines 2 and 7 are examples of this. (e) Image of a cylindrical target as in previous images, except that the continuous lines are substituted by radial arrays of dots; in this case the test surface is a real human cornea. (f) Detail of image in (e), with straight red lines to show the Skew Ray Error on the real cornea.

In Fig 5, the image of a cylindrical target whose axis of symmetry is the z-axis, with concentric rings and straight lines parallel to the z-axis was captured by reflection on a spherical steel ball; the optical axis of the camera lens is also along the z-axis. When the sphere is at the center of the cylinder, the image of the target obtained by reflection on the sphere, is a collection of concentric circles and radial lines; in this case, the chief ray emerging from any point on the target is included in the meridional plane that contains the point (Figs 5(a) and (b)). In Fig 5, the image of a cylindrical target produced by reflection on a spherical steel ball is shown. The optical axis of the camera is *z*; this is also the axis of symmetry of the target which is composed of a set of concentric rings and straight lines parallel to the z-axis. When the sphere is at the center of the cylinder, the image of the target obtained by reflection on the sphere, is a collection of concentric circles and radial lines; in this case, for every point on the target, the chief ray is a meridional ray (Figs 5(a) and (b)). For the same sphere, however, if it is decentered from the z-axis, the image is no longer a set of concentric and radial straight lines (Figs 5(c) and (d)), because the system has lost the symmetry of revolution; then, a chief ray is not a meridional ray anymore, with exception of those rays originating at points of the target located on the symmetry plane containing both the z-axis and the center of the sphere. This means that tracing a ray starting on some point of the target, being reflected on the sphere and arriving at the image sensor of the camera, cannot be only done along a meridional plane of the surface; it is a skew ray, except for those points contained in the meridional plane containing the z-axis.

Several authors have realized that one possible way to overcome the skew ray problem is to use a different target; instead of the classical set of rings as the Placido's disk, a way to identify without ambiguity some points on the target and their corresponding image points. A simple way to do that is to add a set of radial lines to the set of rings, whose intersecting points offer the desired points which can be easily associated with the intersection of the corresponding lines on the image as shown in Fig 5; as far as we know there is no commercial or even experimental device using this proposal; a similar idea was proposed by Schwiegerling [16], with a target composed of two sets of curved lines like hyperbolas producing a squared array of straight lines on the image; the rhomboidal areas between four lines were filled with black and white colors. This target called a 'distorted checkerboard' allowed to overcome the skew ray problem by identifying the corners of the black or white areas on the target and correctly associated with their corresponding corner on the image. Mejía-Barbosa [12] produced a set of almost point sources inside its ovoidal target by strategically locating the final tip of optical fibers conducting the light from a white source to the target surface. Diaz-Uribe [17] used a cylindrical target with a printed target composed of black spots on a white paper and Sicam [18,19] used a set of colored leds in a tight packing along a cone as a target. Maybe one of the most interesting advances was made by Gómez-Tejada [20], they described an iterative method for evaluating a general surface, not necessary with symmetry of revolution, with the classical target of concentric rings; their proposal was not limited to a meridional plane overcoming the skew ray error without using an additional set of lines or individual points on the target.

5 Null-screen method

Since the initial proposals for evaluating the anterior surface of the cornea using the Placido's disk, many authors realized that a set of equally spaced concentric rings produced a set of variable separated curves on the image. In trying to compensate this, for having a more uniform spacing between the sampling points on the cornea, non-equally spaced rings on the target were proposed. For targets composed of individual points, the work of Schwiegerling and Miller [16] seems to be the first with a null screen proposal. The distorted checkerboard target that they proposed was designed to produce a perfect squared checkerboard image on an ellipsoidal surface like the corneal surface with a radius of curvature of 7.8 mm and a conic constant of –0.25. Any deviation of this perfect image was due to a surface deformations or misalignments; in this sense, this was a null screen design. In that work little insight about the design of the distorted checkerboard target was explained.

The first mention as the null-screen method was made by Díaz-Uribe and Campos-García [17], they defined it as a set of lines or dots that are printed on a paper or any other surface. This technique emerged as a novel method for testing optical surfaces. Now, the testing of the optical surfaces using the null-screen method is based on the analysis of the experimental image obtained; this image comes from a set of dots or lines, that are drawn on a screen. The screen can take different shapes, for instance: flat screen, cylindrical screen, conical screen, or whatever chosen geometry. The observed image is formed by reflection on the surface under test, it becomes a perfect pattern (mesh of lines, square or radial arrangement of circles, etc.), as long as the test surface is perfect and located in the appropriate position according to the design parameters (hence the name null-test, since when there are no deformations on the surface, the deviation of the points is zero) [17]. On the contrary, if the position deviations of the points in the resulting pattern image are not null, then, these will be due to imperfections or misalignment of the test surface.

The advantage of the null-screen method for the testing of optical surfaces is that it does not require a purpose-designed optical system for surface evaluation; it only needs a conventional optical system that allows to be viewing the virtual image of the points on the null-screen generated by the reflection on the surface under test. Another feature is that it allows the entire surface to be tested at once. In addition, the lighting used can come from extended light sources, such as fluorescent lamps, or from some other device that emits its own light; an example of this is LCD digital frames, in this way, it is not necessary to have a source with coherent lighting.

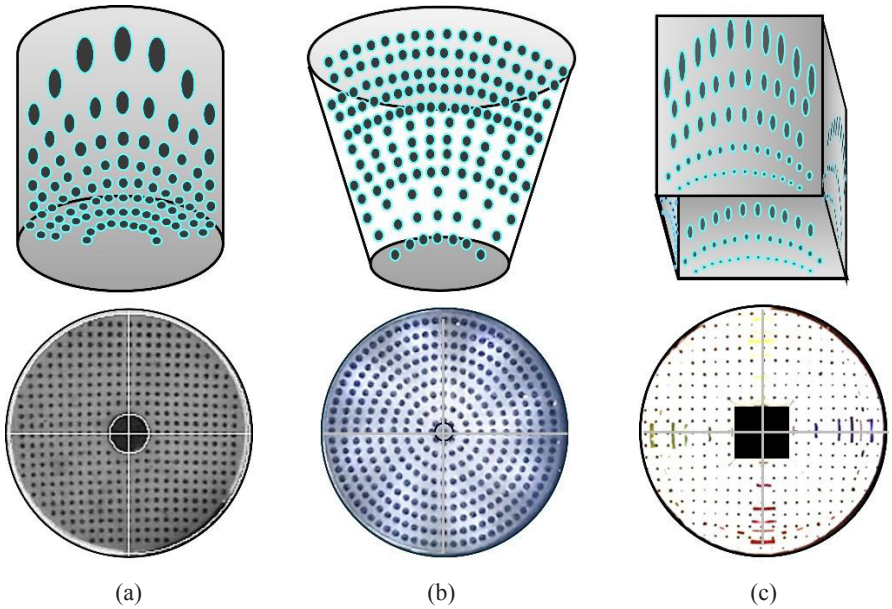

Fig 6. Schematic Null-screens in different geometries with their correspond experimental image obtained after evaluation: (a) Cylindrical null-screen, (b) Conical null-screen, (c) Flat null-screens into a quadrangular prism.

The traditional system of the null-screens method [17] for testing an optical surface is composed of an optical focusing system, a CCD sensor (CMOS or any type of known image detection system), a stop diaphragm, and a cylindrical null-screen (or whatever geometry is proposed). In addition, the null display design proposed here gives an almost flat image, suitable for common optical systems used as image sensors (see section 3. Field curvature). Furthermore, the use of the null-screens method is not restricted only to

the testing of fast aspheric convex surfaces but said method has been widely demonstrated for measuring deformations of a large number of optical surfaces, which include concave and convex surfaces of different sizes [21-25], even surfaces without revolution symmetry, such as off-axis ones [26,27], and in the last years it has been a good choice for testing freeform surfaces [28-31]. It is important to note that the optical system may introduce a small amount of distortion that will need to be considered to correct the experimental results for the (x, y) coordinates of the centroids obtained from the experimental image.

Null-screen method has been used to test aspherical fast convex surface by the implementation of a target in a cylindrical [17], conical [32], or even flat null-screens in an triangular or square prism array parallel to the optical axis, instead of orthogonal to it [33,34] as shown in Fig 6.

6 Design of null-screens

The targets used for measuring the corneal topography, evolved from the Placido´s disk composed of a set of concentric B&W rings on a flat surface orthogonal to the optical axis, which produced a set of rings on the image. Gullstrand [2] realized that an adequate definition of the spacing between the rings on the target can produce an image with almost equally spaced rings. In the radial direction, this proposal was a kind of null screen indeed. Schwiegerling and Miller [16], designed the distorted checkerboard target, the first two dimensional null-screen on a plane orthogonal to the optical axis of the camera; Díaz-Uribe [17], designed a null screen on a cylindrical surface and Mejía-Barbosa and Malacara-Hernández [12] on an ovoidal surface. Díaz-Uribe and Campos-García [35] proposed a more general scheme for designing null-screens. For the design, a well known camera is used; the focal length, the principal planes and the stop and pupil positions of the lens, as well as the size and resolution of the image sensor, must be known. First of all, a set of image points must be defined; usually, a regular array of square or radial distribution of points are used, but even a known image can be used as it has been shown by Aguirre-Aguirre *et al* [28]. For the design, an analytical function representing the surface under test must be used, and the shape of the surface that will be used as a target must be known. An exact ray tracing in reversed order is done; starting on one image point, the straight line passing through the center of the camera lens stop defines the reflected ray; the intersection of this ray with the test surface gives the incidence point on this surface. Applying the vector form of the Refraction Law each incident ray is found and its intersection with the screen surface defines the corresponding object points [Fig 7(a)].

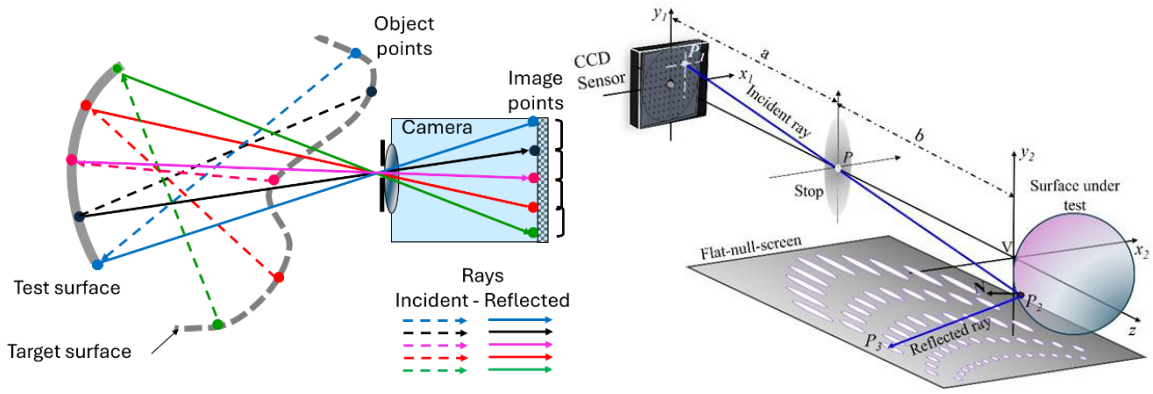

Fig 7. (a) General scheme for designing a null-screen. (b) Example of the three-dimensional ray tracing diagram for the design of a planar null-screen parallel to the optical axis.

As an example, in Fig 7(b) the ray tracing for designing the null screen on a plane parallel to the optical axis is depicted. The objective is to determine the coordinates (x_3, y_3, z_3) which produce a square arrangement of points on the image plane defined by coordinates (x_i, y_i), for measuring the corneal topography with a spherical cornea as a model. A ray starting at the point $P_1 = (x_1, y_1, -b-a)$ is traced towards the nodal point $P = (0, 0, -b)$, where a, is the distance from the aperture stop to the CCD, b is the distance from the aperture stop to the vertex V of the surface. Subsequently, the ray goes to the optical surface under test at the point $P_2 = (x_2, y_2, z_2)$; after the reflection, the ray is redirected towards the plane null-screen and arrive at point $P_3 = (x_3, y_3, d)$; d is the distance from the plane to the optical axis z. With this procedure, an object point is obtained for each image point. Usually, the image is defined as a collection of circular spots, instead of single isolated points; the corresponding object spots are similar to ellipses but in some cases is evident that they are distorted. A complete description of this task is shown in the works reported by Campos-García [23-25] and Rodríguez-Rodríguez [34,37-39].

For this calculations, it is assumed that only one ray is passing through the stop; in this sense the image of each object point is an image point (Fig 8). In practice, however, optical aberrations of the camera lens spread the light at each point, producing a wider light spot. For aberrations depending on the size of the aperture stop, for instance spherical aberration, coma and astigmatism, they can be minimized by closing the stop as far as possible; even for a small stop such as an F/16 aperture, distortion still remains because it depends only on the object's position. Then, it becomes necessary to calibrate the camera lens distortion, to compensate its effects during the calculations. Recent work on calibration of distortion and how it evolves as the object changes its position can be found in a paper by Mejía and Díaz-Uribe [40].

7 Evaluation methods

As it was stated in section 2, the basic principle for a quantitative evaluation of the cornea, is based on the queratometric method for measuring the radius of curvature. Two approximations are used for it, the paraxial theory which is valid only very near the apex, and the solution to the skew ray problem described in section 4. In 1896 Gullstrand [2] developed a non-paraxial theory and was able to get a better approximation to the true shape of the cornea. Different authors made improvements to the non-paraxial method, but the skew ray problem persisted until the work of Schwiegerling [16] who used Zemax (a commercial optical design software), to trace the rays on the system and by optimization found the geometric properties (such as radius of curvature, and position), of the surface producing the image captured by the camera. A similar method was proposed by Aguirre-Aguirre [41], but they used a null screen with drop shaped spots as a target and a randomized algorithm, to find the surface that better reproduces the position of the centroids of the spots in the image. They showed through simulations and experiments the feasibility of the method with spheres and conic surfaces whose radius of curvature, conic constant and 3D vertex position are randomly and strategically varied to find the best surface. In addition, other randomized variables included in the algorithm, are the image and vertex to lens distances.

Indeed, the quantitative evaluation of the cornea can be described generally as follows. All the specular reflection methods use a target with a well-defined geometry and a camera to capture an image of the target produced by reflection on the cornea to be measured. So, the position of every point of the target and its corresponding image on the camera sensor are well known. The goal of the method is to find the exact point on the anterior corneal surface where the chief ray is reflected, for each point of the target. The problem seems to be simple, but its solution can only be obtained in an approximated way and after some iterative procedure better approximations are obtained successively, thus a good enough approximate solution can be obtained.

All the evaluation methods use the pinhole model of the camera; then, the reflected ray can be easily obtained as the straight line joining the image point and the pinhole, the center point of the camera

lens stop. The corresponding incident ray cannot be obtained a priori because only the point on the target is well known, no other point on this ray is known. The exact incidence point on the cornea is unknown, so it cannot be used. A first approximation to the incidence point is obtained from an analytical expression approximating the corneal surface, which is called the reference surface; the intersection point between the reflected ray and the reference surface is used as the incidence point, so the straight line joining this point and the corresponding point on the target gives a first approximation to the incident ray. A natural proposal to the reference surface is a spherical surface but even a plane surface is a good start. Of course, the incident points thus obtained are not the solution to our problem, because they are on the reference surface but no on the test surface. The key point is that the true test surface is that one which satisfies the law of reflection at every incidence point. The law of reflection involves the incident and reflection angles relative to the normal to the surface, and this normal is given by the gradient of the surface function. This yields a differential equation for the points on the surface.

Mejía and Galeano [42], recognized that the image spot pattern is similar to the Hartmann Test for astronomical telescopes so they used some differential equations similar to the Rayces Equations [43] to obtain the shape of the cornea. They applied the Fourier method to integrate the differential equation which is a kind of modal method. Snellenburg *et al* [44], wrote the differential equation in a somewhat different way and proposed an iterative method called Forward Ray Tracing to obtain the shape of the surface; they showed that after few iterations the method converges to a better solution, than obtained through other methods.

Díaz-Uribe and Granados-Agustín [45,46] proposed a different kind of an experimental corneal topographer. It was based on an unexpanded laser beam scanning the corneal surface, in such a way that the beam was always directed to a fixed point coincident with the center of curvature of the apex of the cornea; the reflected beam was monitored by a position sensing detector, so that the incident and the reflected beams were well known every time. With this information, the normal to the surface at each incidence point can be computed by using the vector form of the Reflection Law of the Geometrical Optics,

$$\vec{N} = \hat{R} - \hat{I} \tag{5}$$

This proposal was abandoned because of technological limitations meaning that it was too complex to scan the cornea in less than 10 ms to freeze the corneal movements. At the time it was also impossible to implement some kind of eye tracker to compensate these eye movements during the measurement The most important product of the proposal was a general exact equation to obtain the incident points $\vec{r}$ on the surface, which gives the shape of the surface, from the normal $\vec{N}$ and the path described by its tangent vector $\vec{ds}$,

$$\vec{N}(\vec{r}) \cdot \vec{ds}(\vec{r}) = 0 \tag{6}$$

This is a differential equation for vector $\vec{r}$ in 3D, which has neither limitation to the paraxial zone of the surface, nor to meridional planes. Later, Díaz-Uribe [47], proposed to use it for the Null-Screen method applied for the measurement of the segments of the Large Millimetric Telescope and wrote a solution in cartesian coordinates which reads as follows

$$z - z_0 = -\int_{(x_0, y_0)}^{(x, y)}_{\mathscr{C}} \left(\frac{N_x}{N_z} dx + \frac{N_y}{N_z} dy \right), \tag{7}$$

where (N_x, N_y, N_z), are the cartesian coordinates of the normal vector, (x, y, z) and (x_o, y_o, z_o), are the last and the initial points of an integration path $\mathscr{C}(x, y, z)$; dx and dy are the corresponding components of the

differential vector tangent to the path. Essentially, the representative point for each spot at the image is associated with the centroid of its intensity distribution. Starting at this point, the reflected ray $\vec{R}$ at the surface is obtained as the straight line passing through the pupil of the camera lens. The incidence point is unknown because it lies on the surface to be evaluated. Assuming that the real surface is not far from some theoretical surface, which is called the reference surface, a good guess to the incident point is obtained by intersecting the reflected ray with this surface. The incident ray $\vec{I}$ is then approximated by the straight line joining the approximated incidence point and the corresponding point on the spot at the target. Having these two rays, the unit incident and reflected vectors are calculated and the corresponding normal is obtained with Eq (5). The cartesian components of this vector are substituted in Eq (6) to obtain the shape of the surface. Even though Eq (6) have no approximations, the evaluation of the normal vector is only approximated and is obtained only in a discrete collection of incident points, so a numeric method must be used to evaluate the integral in Eq (7). A way to improve the normal approximation is to use an iterative method where the first approximated evaluation of the surface is used as the new reference surface for a second evaluation, the second evaluation is used for the third one and so on. Numerical simulations of this procedure have shown that a good guess for the first surface can be sufficient in many cases, but when the iterative algorithm is used, the result is almost insensitive to the first guess of the surface. For the iterative procedure, it is more important to make a good choice for the initial vertex position of the surface along the z axis. Another iterative method can be used to find the optimum value for this position, as well as for transversal decentering of the surface.

Another important issue of the integration methods is the fact that the integral is a path integral, so that different paths can be chosen to find the sagitta z value at some end point. In addition, the integrand in Eq (7) is given by the x and y components of the normal divided by the z component. For discrete points, however, which are only a finite sample of the points on the image plane, the integral is dependent on the path followed during the integration procedure. This is true even for equally spaced points, so, even for the Hartmann test, the result of the integral can have clear variations for different integration paths, as noted by Ghozeil [48].

Maybe it is not a surprise that Eq (7) is very similar to the solution of the Rayces Equations [43], for obtaining the wavefront aberrations from the transversal ray aberration. There are, however, significative differences between both equations; the first and more evident is that Rayces Equations are useful for measuring wavefront aberrations, whereas Eq (7) are used to obtain the shape of the surface; it is true, that these two concepts are closely related, but are not the same. When a wavefront is reflected on a surface, the properties of the reflected beam are due both, to the kind of incident wavefront and to the shape of the surface where the beam is reflected; as far as we know there is not a general equation relating, the wavefront and the reflecting surface. For simple cases, as the reflection of a plane wave on a flat surface, the wavefront aberration is twice the surface deformations [49]. In practice, integration in Eq (7) is similar to integration of the Rayces Equations, so the same methods can be used. Usually these methods are applied to the Hartmann Test, some of them are described by Malacara-Doblado [50]. Usually, these methods are classified as zonal or modal integration methods; the first class refers to those methods which are applied to one or few points at a time, and then are sequentially applied to all the points whereas the second class is applied to all the evaluation points at once by fitting a set of functions to the evaluation points.

The most simple, but powerful, method is the trapezoidal integration method which belongs to the class of zonal methods. This method has been widely used for the Hartmann test. When the Hartmann screen is composed of a square array of holes, the integration is carried out along the directions of the distribution of holes on the screen, and in this case differentials dx and dy in the integral are substituted by a constant value d (the separation of the holes in the x and y directions), and this term can be factorized out on the integrals in each direction. When this method is applied to the Null-Screen Method, however, the

integration is made along the evaluation points located at the incident points on the surface; these points are obtained from the spots of the captured image, so they are not equally spaced, except when the test surface for which the null screen was designed is perfect without deformations or misalignments. Then the distance between two adjacent points which represent the x and y differentials, cannot be factorized; the corresponding equations are a little more complex, but they remain very simple. The sagitta at some final point numbered by the subindex $i + 1$, is computed by using the normals quotients and the x, y coordinates at each incident point along some defined path through equations deduced by Campos-García [23] when they tested an f/0.23, ellipsoidal surface, 164 mm in diameter, as follows:

$$z_{i+1} = z_o - \sum_{j=0}^{i} \left\{ \left(\frac{N_{xj}}{N_{zj}} + \frac{N_{x(j+1)}}{N_{z(j+1)}} \right) \frac{(x_{j+1} - x_j)}{2} + \left(\frac{N_{yj}}{N_{zj}} + \frac{N_{y(j+1)}}{N_{z(j+1)}} \right) \frac{(y_{j+1} - y_j)}{2} \right\} \tag{8}$$

The sagitta z_o of the starting point must be known in advance; starting at the same initial point for every path, it has a constant value, which can be defined as zero, without changing the shape of the surface; it only adds a piston term.

There are other zonal integration methods, e.g. one of the most well-known is the Southwell Algorithm [51], which uses the trapezoidal method when one point is approached from the nearest neighbors along each of the four x, y paths and then average the four different values. This procedure smooths the different values obtained along each single path, but there is no guarantee that the result is the best. This method was proposed [51] for the Hartmann Test with a square array of holes on the Hartmann screen; it can be applied to the null screen method for measuring different surfaces including the cornea, provided that Eq (8) is used instead of equations deduced for equally spaced points in a squared array too. A similar procedure can be devised for other x, y distributions of measured points, such as radial, spiral or triangular arrays.

The modal integration procedures propose an integrated function $z(x, y)$ as a linear combination of n functions $G(x, y)$ as

$$z = f(x, y) = \sum_{j=1}^{n} A_j \, G_j \, (x, y) \tag{9}$$

where, the coefficients A_j are constants to be determined by the measured normals by using Eq (10).

$$\vec{N}(x, y) = \nabla[f(x, y) - z] = \sum_{j=1}^{n} A_j \left[\frac{\partial G_j \, (x, y)}{\partial x} \, \hat{i} + \frac{\partial G_j \, (x, y)}{\partial y} \hat{j} - \hat{k} \right] \tag{10}$$

or, by components

$$N_x(x, y) = \sum_{j=1}^{n} A_j \frac{\partial G_j \, (x, y)}{\partial x},$$

$$N_y(x, y) = \sum_{j=1}^{n} A_j \frac{\partial G_j \, (x, y)}{\partial y},$$

$$N_z(x, y) = -\sum_{j=1}^{n} A_j, \tag{11}$$

which must be satisfied at every one of the m evaluation points. Then we get a set of $3m$ linear equations with n unknown coefficients A_j, which can be solved by a least-squares fit. The key point here is that usually m is larger than n, the matrix of the linear system is not square, so a proper numeric method, such as the

Singular Valued Decomposition method (SVD) or the Levenberg–Marquardt algorithm, must be used to solve it. A detailed explanation of these methods are out of the scope of this paper, but some of these methods are described in the well known reference [52] and are implemented in most of the specialized software. The result of solving Eq (11), is the set of n A_j values, and by substituting in Eq (9) an analytical representation of the surface to be evaluated is obtained. One of the most common choices for the $G_j(x, y)$ functions is the Zernike polynomials [53], which are a basis for the functions defined over a unit circle domain. Common representations of the the Zernike polynomials as in ref [53], are defined for a continuous domain; for a set of discrete points over a domain, however, the Zernike polynomials are no longer orthogonal, but the Gram–Schmidt process of linear algebra can be applied to get a specific orthonormal representation of Zernike type polynomials over a defined distribution of evaluation points on a domain. Some examples of them were deduced by Hernández-Gómez *et al* [54].

8 Topographers based in null-screens

The early literature on the design of null-screens with the intention of implementing keratometry was the work carried out by Funes-Maderey and Díaz-Uribe [55] and Colín-Flores and Díaz-Uribe [56]. These works emphasize the use of the null-screens to evaluate an aspherical simulator with the dimensions close to the human cornea. The work of Funes-Maderey and Díaz-Uribe [55] shows a qualitative analysis of the evaluation of a corneal surface using cylindrical null-screens of lines of different thicknesses, which generate an image of concentric rings in the cornea, reproducing in this way, an image like the formed by the Placido disk system. The work of Colín-Flores and Díaz-Uribe [56] showed quantitative results of the evaluation of the corneal surface of an adult using a cylindrical null-screen with drop shaped spots to produce circular spots on the image; in addition, they reproduced the Ludlam and Wittenberg [11] calculations and demonstrated the feasibility of using cylindrical screens with the idea of having an object surface that can generate a flatter image. More recently, Estrada-Molina [57] resumed the design of a cylindrical null-screens in order to build a portable topographer for measuring the cornea of children, elders, and every people with mobility restrictions; with this prototype he performed some quantitative evaluations of calibration spheres, to find, in a first approximation, the surface of the human cornea. Finally, the prototype has been implemented and is currently in the validation phase (Fig 8) [58].

Fig 8. (a) Portable topographer TOCO based on a cylindrical null-screen, (b) Testing the human cornea of an informed subject.

Other kind of experimental topographers have been the implemented by Campos-García [59-61], and Peña-Conzuelo [62,63], these authors have proposed a conical null-screen topographer. They have shown its feasiblity for evaluating the human cornea; also, they reported a compact conical topographer based in a null-screen method [64-66] and Huerta-Carranza [67]. With this design, they measured the corneal topography using a mobile device implemented in a smartphone [64-67] (Fig 9).

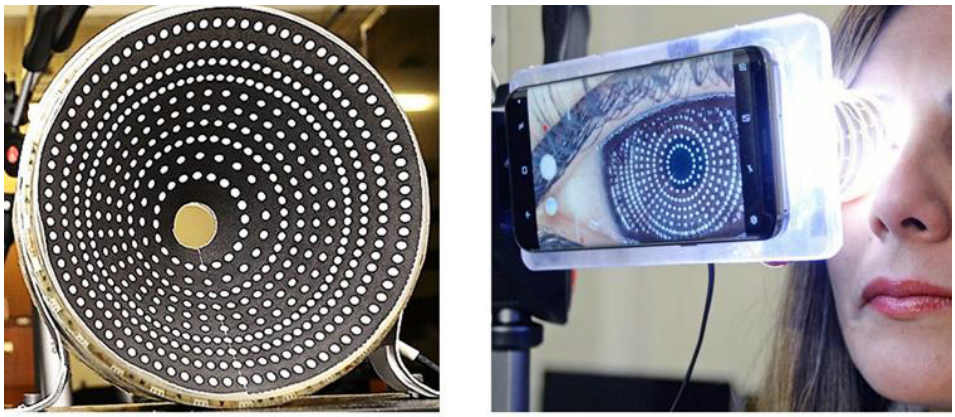

(a) (b)

Fig 9. (a) Experimental Topographer based in conical null-screen. (b) Measurement of the human cornea of an informed subject with a cellphone.

9 Dynamic Point Shifting Method

The Point Shifting method (PoS), was proposed for the first time by Moreno-Oliva *et al* [21] and developed further by Moreno-Oliva *et al* [22]. In these works, the evaluation of a fast concave aspheric surface was performed. Then, the same authors [24], proposed applying a dynamic version (DyPoS) of the method on fast convex surfaces of greater dimensions (around 60 mm) using four LCD screens as targets. The DyPoS method consists of changing the position of the spots on the LCD's several times and getting a new experimental distribution of object spots each time, thus changing the image spots for each position. This method increases the density of the evaluation points on the surface under test, increasing accordingly the lateral resolution of the measurement and reducing in this way the truncation errors in the numerical integration procedure.

The truncation error for the trapezoidal integration method is reduced to ε/η, where ε is the truncation error for a single image evaluation, and η is the number of shifts and captured images of the spots [21,22,24,33]. A set of three plane LCDs can be used as an approximation to a cylindrical target, to reduce the field curvature. To produce a square array of spots on the image, each of the three LCDs needs a different null-screen design. They were able to show a reduction in the truncation error during the integration by the trapezoidal rule method [33]. This proposal significantly improved the image quality and reduced the truncation error further. For the DyPoS a different null screen must be designed for each step, which also avoids mechanical movements of some parts of the setup. To implement this idea in a corneal topographer, a very different kind of target was proposed by Rodríguez-Rodríguez [37,38,68] with a null-screen in a triangular prism configuration composed of three flat null-screens. In this case, they used LCD photo frames in order to display the null-screens. One of the main advantages of this configuration is that any distribution of spots can be designed without moving the experimental configuration. Possible distributions include square and radial arrays of black spots on a white background on the image or even with reversed contrast. Colored spots were used to simplify the correspondence between the object and image spots, even if the spots are close to each other. The number, size and shape of the spots on the image plane can also be varied. A somewhat different proposal was an array of four flat-null-screens in a quadrangular prism configuration which was patented in 2021 [69]. The first results with this target configuration and applying the DyPoS with calibrated spheres were reported by Valderrama-Juárez & Díaz-Uribe [70]. They used four flat OLED screens instead of three LCD with the advantages of being able to design and display the same

array of spots on the four OLEDs. In addition, the OLEDs overcome the limitations of deep contrast changes of LCDs for different viewing angles, resulting in difficulties to process the image to find the centroid of different spots. Rodríguez-Rodríguez *et al* [71], made additional improvements to this configuration by adding LEDs of different colors and with variable intensities, as a sentinel to identify each of the screens without ambiguity. A second set of LEDs were placed at the edges of the prism formed by the LCD, and a third set of LEDs in a square matrix was placed on the base of the quadrangular prism in the direct field of view of the camera. These two sets of LEDs eliminate the blind areas where there are no evaluation spots because of the frames of the OLED screens and the hollow prism end causing missing spots at the center of the pattern. With these modifications the number of evaluation points is increased and the blind zones are reduced a great deal, allowing a better sampling of the optical surface under study. In a recent work Rodriguez-Rodriguez [34], used the same configuration with static flat screens. They showed experimental results with calibrated spheres as well as with an informed volunteer. These ideas are shown in Fig 10.

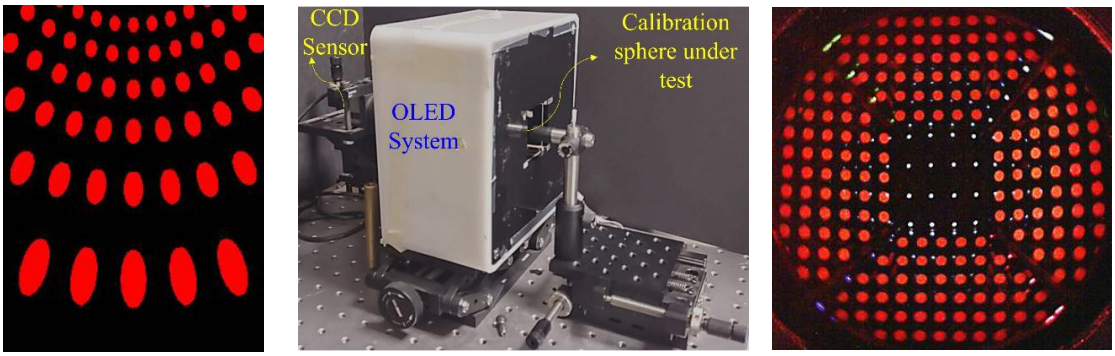

(a) (b) (c)

Fig 10. Topographer based in Dynamic Point Shifting Method by OLED System, (a) Dynamic null-screen, (b) OLED Prism Configuration and LEDs sources, (c) Image captured with the DyPoS in a quadrangular prism Null-screen target.

In this way, we can notice that the null-screen method includes different screen designs with also different geometries, where, of course, each configuration has its advantages and disadvantages.

10 Conclusions

In this paper, two of the main problems related to the early specular topographers have been described, they are the field curvature and the skew ray problems; main references to this matter are listed for better understanding and study. Also, the so called Null-screen testing methods and how they solved the main problems were described. Further, recent developments of this method were documented including different target configurations, the design of the null screen and the most used method to quantify the shape of the human cornea. The Null Screen method for a quantitative evaluation of the corneal topography has demonstrated to be a very efficient tool for knowing the shape of the anterior corneal surface for different applications including the fitting of rigid contact lens.

Acknowledgements

The research described in this publication was made possible in part by PAPIIT grants from DGAPA-UNAM IT103823, IA106823. Also, the support by SECIHTI (LaNOV, grant number LNC-2023-121) is recognzed.

References

1. Levine J R, The true inventors of the keratoscope and photo-keratoscope, *Br J Hist Sci*, 2(1965)324–342.
2. Gullstrand A, Photographic-ophthalmometric and clinical investigations of corneal refraction, *Optom Vis Sci*, 43(1966)143–197.
3. Koch D D (1992), Wakil J S, Samuelson S W, Haft E A, Comparison of the accuracy and reproducibility of the keratometer and the EyeSys Corneal Analysis System Model I, *J Cataract Refract Surg*, 18(1992)342–347.
4. Eyesys (2024); http://eyesys.com/products/desktop.html.
5. Atlas (2024); https://www.zeiss.com/meditec/en/products/zeiss-corneal-topographers/zeiss-atlas-500-corneal-topographer-us.html.
6. Cornea (2024); https://www.essilor-instruments.com/product-cornea-550/.
7. Cairns G, McGhee CNJ, Orbscan computerized topography: Attributes, applications, and limitations, *J Cataract Refract Surg*, 31(2005)205–220.
8. Pentacam; https://www.pentacam.com/int, (2024).
9. Mohammadpour M, Heidari Z Pentacam, In: Mohammadpour M (ed), Diagnostics in Ocular Imaging, (Springer), 2021.
10. Dorronsoro C, Pascual D, Pérez-Merino P, Kling S, Marcos S, Dynamic OCT measurement of corneal deformation by an air puff in normal and cross-linked corneas, *Biomed Opt Express*, 3(2012)473–487.
11. Ludlam W M, Wittenberg S, Measurements of the ocular dioptric elements utilizing photographic methods. Part II. Cornea-Thoretical considerations, *Optom Vis Sci*, 43(1966)249–267.
12. Mejía-Barbosa Y, Malacara-Hernández D, Object surface for applying a modifed Hartmann test to measure corneal topography, *Appl Opt*, 40(2001)5778–5786.
13. El Hage S G, A New Conception of the Corneal Topology and Its Application, *Optica Acta: Int J Opt*, 19(1972)431–433.
14. Klein S A, Axial curvature and the skew ray error in corneal topography, *Optom Vis Sci*, 74(1997)931–944.
15. Applegate R A, Howland C H, Noninvasive Measurement of Corneal Topography, IEEE Engineering in Medicine and Biology Magazine, 14(1995)30–42.
16. Schwiegerling J, Miller J M, A Videokeratoscope Using a Distorted Checkerboard Target, in Vision Science and its Applications, Technical Digest Series, (Optica Publishing Group, 1998), paper MA.4.
17. Díaz-Uribe R, Campos-García M, Null-screen testing of fast convex aspheric surfaces, *Appl Opt*, 39(2000)2670–2677.
18. Sicam V A, van der Heijde R G. Topographer reconstruction of the nonrotation-symmetric anterior corneal surface features, *Optom Vis Sci*, 83(2006)910–918.
19. Sicam V A, Snellenburg J J, van der Heijde RG, van Stokkum I H, Pseudo forward ray-tracing: a new method for surface validation in cornea topography, *Optom Vis Sci*, 84(2007)915–923.
20. Gómez-Tejada D, Malacara-Hernández Z, Malacara-Doblado D, Malacara Hernández D, Zonal integration of circular Hartmann and Placido patterns with nonrotationally symmetric aberrations, *J Opt Soc Am A*, 37(2020)1381–1389.
21. Moreno-Oliva V I, Campos-García M, Bolado-Gómez R, Díaz-Uribe R, Point shifting in the optical testing of fast aspheric concave surfaces by a cylindrical screen, *Appl Opt*, 47(2008)644–651.
22. Moreno-Oliva V I, Campos-García M, Díaz-Uribe R, Improving the quantitative testing of fast aspherics with two-dimensional point shifting by only rotating a cylindrical null screen, *J Opt A: Pure Appl Opt*, 10(2008)104029; doi.10.1088/1464-4258/10/10/104029.
23. Campos-García M, Bolado-Gómez R, Díaz-Uribe R, Testing fast aspheric concave surfaces with a cylindrical null screen, *Appl Opt*, 47(2008)849–859.
24. Moreno-Oliva V I, Campos-García M, Granados-Agustín F S, Santiago-Alvarado A, Díaz-Uribe R, Improving fast aspheric convex surface test with dynamic null screens using LCDs, *Appl Opt*, 50(2011)3101–3109.
25. Campos-García M, Díaz-Uribe R, Granados-Agustin F S, Testing fast aspheric convex surfaces with a linear array of sources, *Appl Opt*, 43(2004)6255–6264.

26. Avendaño-Alejo M, Díaz-Uribe R, Testing a fast off-axis parabolic mirror using tilted null-screens, *Appl Opt*, 45 (2006)2607–2614.
27. Avendaño-Alejo M, Moreno-Oliva V I, Campos-García M, Díaz Uribe R, Quantitative evaluation of an off-axis parabolic mirror by using a tilted null-screen, *Appl Opt*, 48(2009)1008–1015.
28. Aguirre-Aguirre D, Villalobos-Mendoza B, Díaz-Uribe R, Manuel Campos-García, Null-screen design for highly freeform surface testing, *Opt Express*, 28(2020)36706–36722.
29. Gonzalez-Utrera D, Aguirre-Aguirre D, Rodríguez-Rodríguez M I, Díaz-Uribe R, Null-screen testing of the complementary freeform surfaces of an adjustable focus lens, *Opt Express*, 29(2021)21698–21710.
30. Gonzalez-Utrera D, Aguirre-Aguirre D, Díaz-Uribe R, Alternative Method to Design Null-screen for testing Freeform Surfaces, Frontier in Optics/Laser Science, Lee B, Mazzali C, Corwin K, Jason Jones R J, (eds), OSA Technical Digest (Optica Publishing Group, 2020), paper FM1A.4.
31. Gonzalez-Utrera D, Villalobos-Mendoza B, Diaz-Uribe R, Aguirre-Aguirre D, Modeling, fabrication, and metrology of 3D printed Alvarez lenses prototypes, *Opt Express*, 32(2024)3512–3527.
32. Campos-García M, Cossio-Guerrero C, Moreno-Oliva V I, Huerta-Carranza O, Surface shape evaluation with a corneal topographer based on a conical null-screen with a novel radial point distribution, *Appl Opt*, 54(2015)5411–5419.
33. Rodriguez-Rodríguez M I, Jaramillo-Nuñez A, Díaz-Uribe R, Dynamic point shifting with null screen using three LCDs as targets for corneal topography, *Appl Opt*, 54(2015)6698–6710.
34. Rodriguez-Rodríguez M I, Gonzalez-Utrera D, Aguirre-Aguirre D, Vohnsen B, Díaz-Uribe R, Corneal topographer using null-screen patterned within a quadrangular acrylic prism, *Opt Continuum*, 3(2024)36–50.
35. Díaz-Uribe R, Campos-García M, Medium Precision Geometrical Test for Very Fast Aspheres, in Frontiers in Optics, OSA Technical Digest (CD) (Optica Publishing Group), 2006, paper OFTuA1.
36. Aguirre-Aguirre D, Campos-García M, Díaz-Uribe R, Villalobos-Mendoza B, General equations for the null-screen test for aspherical surfaces with deformation coefcients, *Appl Opt*, 57(2018)10230–10238.
37. Rodríguez-Rodríguez M I, Método de corrimiento dinámico de puntos en queratometría por pantallas nulas, Ph D Thesis, Instituto Nacional de Astrofísica Óptica y Electrónica, México, (2015).
38. Rodriguez-Rodríguez M I, Jaramillo-Nuñez A, Díaz-Uribe R, Dynamic point shifting with null screen using three LCDs as targets for corneal topography, *Appl Opt*, 54(2015)6698–6710.
39. Rodríguez Rodríguez M I, Valderrama-Juárez C E, Damián-Zamacona J R, Díaz-Uribe R, Corneal topography using Dynamic point shifting method in quadrangular OLED prism, 2022; Proc SPIE Vol 12221: 122211C 1-10.
40. Mejía Y, Díaz-Uribe R, Third order distortion analysis from an envelope curve, *Opt Commun*, 454(2020)124492; doi.org/10.1016/j.optcom.2019.124492.
41. Aguirre-Aguirre D, Diaz-Uribe R, Campos-Garcia M, Villalobos-Mendoza B, Izazaga-Pérez R, Huerta-Carranza O, Fast conical surfaces evaluation with null-screens and randomized algorithms, *Appl Opt*, 56(2017)1370–1382.
42. Mejía Y, Galeano J C, Corneal topographer based on the Hartmann test, *Optom Vis Sci*, 86(2009)370–381.
43. Rayces J L, Exact Relation between Wave Aberration and Ray Aberration, *J Mod Opt*, 11(1964)85–88.
44. Snellenburg J J, Braaf B, Hermans E A, van der Heijde RGL, Sicam VADP, Forward ray tracing for image projection prediction and surface reconstruction in the evaluation of corneal topography systems, *Opt Express*, 18(2010)19324–19338.
45. Díaz-Uribe R, Granados-Agustín F, Theory for Evaluation of the Corneal Shape in Laser Keratopography, in Vision Science and its Applications, Technical Digest Series, (Optica Publishing Group, 1996), paper SuB.1.
46. Díaz-Uribe R, Granados-Agustín F, Corneal Shape Evaluation by Using Laser Keratopography, *Optom Vis Sci*, 76((1999)40–49.
47. Díaz-Uribe R, Medium-precision null-screen testing of off-axis parabolic mirrors for segmented primary telescope optics: the Large Millimeter Telescope, *Appl Opt*, 39(2000)2790–2804.
48. Ghozeil I, Simmons J E, Screen Test for Large Mirrors, *Appl Opt*, 13(1974)1773–1777.
49. Cornejo-Rodriguez A, Ronchi Test, in Optical Shop Testing, Chapter 9, 3rd Edn, (ed) Daniel Malacara, (John Wiley & Sons, Inc.), 2007.

50. Malacara-Doblado D, Ghozei I, Hartmann–Shack, and Other Screen Tests, in Optical Shop Testing, Chapter 10, 3rd edn, (ed) Daniel Malacara, (John Wiley & Sons, Inc,), 2007.
51. Southwell W H, Wave-Front Estimation from Wave-Front Slope Measurements, *J Opt Soc A*m, 70(1980)998–1006.
52. William H, Teukolsky S A, Vetterling William, Flannery B P, Numerical Recipes in C: The Art of Scientific Computing, 2nd edn, (Cambridge University Press, USA), 1992,
53. Mahajan V N, Zernike Polynomials and Wavefront Fitting, in Optical Shop Testing, Chapter 13, 3rd edn, (ed) Daniel Malacara, (John Wiley & Sons, Inc), 2007.
54. Hernández-Gómez G, Malacara-Doblado D, Malacara-Hernández Z, Díaz-Uribe R, Malacara-Hernández D, Modal Integration of Hartmann and Shack-Hartmann Patterns, *J Opt Soc Am A*, 31(2014)846–851.
55. Funes-Maderey I, Díaz-Uribe R, Corneal topography reconstruction by videoqueratometry in three dimensions,1997OSA Annual Meeting, Long Beach. California, EUA. 12 - 17 October,1997. See also: I. Funes-Maderey, Videoqueratometría de campo plano, BSc thesis in Physics, Facultad de Ciencias, UNAM, México, December,1998.
56. Colín-Flores R, Díaz-Uribe R, Análisis de la planicidad de campo para imágenes de pantallas cilíndricas formadas por superfcies esféricas en la aproximación parabasal. XLVIII Congreso Nacional de Física, Sociedad Mexicanade Física, Guadalajara, Jalisco, México, 17-21 October, 2005.
57. Estrada-Molina A, Topografo Corneal Portatil Basado en Pantallas Nulas (Portable Corneal Topographer Based on Null Screens), Ph D Thesis, Universidad Nacional Autonoma de Mexico, México, (2014).
58. https://blepsvision.com/ consulted May 26th, 2024.
59. Campos-García M, Armengol-Cruz V E, Osorio-Infante A I, Evaluating the anterior corneal surface using an improved null-screen system, *OSA Continuum*, 2(2019)736–748.
60. Campos-García M, Aguirre-Aguirre D, Moreno-Oliva V I, Huerta-Carranza O, Armengol-Cruz V de E, Measurement and correction of misalignments in corneal topography using the null-screen method, *OSA Continuum*, 4(2021)158–170.
61. Campos-García M, Pantoja-Arredondo L Á, Aguirre-Aguirre D, Moreno-Oliva V I, Huerta-Carrranza O, ArmengolCruz V E, Measurements of corneal topography using a compact null-screen corneal topographer with a mobile device, Proc SPIE 11873, Optical Fabrication, Testing, and Metrology VII, 118730F (12 September 2021); doi. org/10.1117/12.2592802.
62. Peña-Conzuelo A, Campos-García M, Modeling the conical corneal null-screen topographer with the Fermat principle, Proc SPIE 11352, Optics and Photonics for Advanced Dimensional Metrology, 113521C (1 April 2020); doi.org/10.1117/12.2556053.
63. Peña-Conzuelo A (2020-2), Campos-García M, Aguirre-Aguirre D, Huerta-Carranza O, Analysis of the systematic and random errors in the conical corneal null-screen topographer, Proc SPIE 11352, Optics and Photonics for Advanced Dimensional Metrology, 113521H (1 April 2020); doi.org/10.1117/12.2556056.
64. Campos-García M, Huerta-Carranza O, Pantoja-Arredondo L Á, Cruz-Félix Á S, Santiago-Alvarado A, Aguirre-Aguirre D, Moreno-Oliva V I, Camargo-Fierro C, Conical null-screen design for evaluating a biónic surface using a smartphone-based corneal topographer, Proc SPIE 12221, Optical Manufacturing and Testing XIV, 122210L (3 October 2022); doi.org/10.1117/12.2633701.
65. Campos-García M, Aguirre-Aguirre D, Pérez-Lomelí J S, Peña-Conzuelo A, Huerta-Carranza O, Camargo-Fierro C, Design of a compact corneal topographer to characterize the shape of the cornea, Proc SPIE 11352, Optics and Photonics for Advanced Dimensional Metrology, 113521A (1 April 2020); doi.org/10.1117/12.2556052.
66. Campos-García, Aguirre-Aguirre D, Lechuga-Núñez J A, Peña-Conzuelo A, Design of a null-screen for a compact corneal topographer, *Proc SPIE* 11057, Modeling Aspects in Optical Metrology VII, 110570I (21 June 2019). doi. org/10.1117/12.2526241.
67. Huerta-Carranza O, Campos-García M, Moreno-Oliva V I, Aguirre-Aguirre D, Pérez-Lomelí J S, Smartphone-based corneal topography with null-screens, *Appl Opt*, 61(2022)1381–1388.
68. Rodríguez-Rodríguez M I, Jaramillo-Núñez A, Díaz-Uribe R, Dynamic point shifting in null screen videokeratometry, Proc SPIE 8011: 80119H.2011; 1–8.
69. Díaz-Uribe R (2021), Rodríguez-Rodríguez M I, APARATO MÉTODO Y SISTEMA PORTÁTIL PARA MEDIR LA TOPOGRAFÍA CORNEAL [Portable Apparatus, Method and System for measuring the corneal topography], Mexican Patent 378804, IMPI (10 March 2021).

70. Valderrama-Juárez E, Díaz-Uribe R, Experimental results of a quadrangular OLED prism topographer prototype with Dynamic Point Shifting, in Latin America Optics and Photonics (LAOP) Conference 2022, Technical Digest Series (Optica Publishing Group), paper W3D.4.
71. Rodríguez- Rodríguez M I, Valderrama-Juárez C E, Damián-Zamacona J R, Díaz-Uribe R, Corneal topography using Dynamic point shifting method in quadrangular OLED prism, *Proc SPIE*, 2022; 12221: 122211C 1-10.

[*Received*: 16.06.2024; *rev recd*: 28.06.2024; *accepted*: 29.06.2024]

Rufino Díaz-Uribe obtained the BSc (1980), MSc (1982) and the Ph D (1990) degrees in physics from the National University of Mexico (UNAM). Presently he is at the Institute for Applied Sciences and Technology-UNAM. His main research area is Optical Testing, he developed the Null Screen method for measuring the topography of human corneas and the shape of mirrors used as solar concentrators. In 1996 and 2019 he was honored by the UNAM for his teaching work. He is Senior member of SPIE (2016) and OPTICA (2017). In 2016 he founded Bleps Vision, a startup for developing a portable corneal topographer.

Graduated in Physics from the Benemérita Universidad Autónoma de Puebla (BUAP), Master's and PhD in Sciences in the Specialty of Optics, from the National Institute of Astrophysics, Optics and Electronics (INAOE). Postdoc at the Instituto de Ciencias Aplicadas y Tecnología (ICAT-UNAM) and the University College Dublin UCD, Southern Ireland. He is currently a Full-Time Associate Professor in the Optometry School at FES-Iztacala UNAM. His current research interests are Visual Optics, Corneal Topography, Optical Instrumentation for the evaluation of aspherical and free-form surfaces.

Yobani Mejía-Barbosa is as full-time professor at the Department of Physics at the Universidad Nacional de Colombia, where he has taught courses in optics for more than 15 years. He received his BS and MS degrees in physics from the Universidad Nacional de Colombia in 1991 and 1995, respectively, and his Ph D degree in optics from the Centro de Investigaciones en Óptica, México, in 2001. His current research interests include optical design, interferometry, visual optics, and classical coherence. He is a member of SPIE and a senior member of OPTICA.